Contents lists available at ScienceDirect

Arabian Journal of Chemistry

journal homepage: www.ksu.edu.sa

Original article

Hydroxyapatite incorporated metakaolin/sludge based geopolymer adsorbent for copper ions and ciprofloxacin removal: Synthesis, characterization and mechanisms

Pilomeena Arokiasamy [a,b], Mohd Mustafa Al Bakri Abdullah [a,b,*], Shayfull Zamree Abd Rahim [a,c], Andrei Victor Sandu [d], Anna Fedrigo [e], Ratna Ediati [f], Shafiq Ishak [g], Noor Haida Mohd Kaus [h]

[a] Centre of Excellence Geopolymer & Green Technology (CEGeoGTech), Universiti Malaysia Perlis (UniMAP), 01000 Perlis, Malaysia
[b] Faculty of Chemical Engineering & Technology, Universiti Malaysia Perlis (UniMAP), 01000 Perlis, Malaysia
[c] Faculty of Mechanical Engineering & Technology, Universiti Malaysia Perlis (UniMAP), 01000 Perlis, Malaysia
[d] Faculty of Material Science and Engineering, Gheorghe Asachi Technical University of Iasi, 41 D. Mangeron St., 700050 Iasi, Romania
[e] STFC, Rutherford Appleton Laboratory, ISIS Facility, Harwell OX11 0QX, UK
[f] Faculty of Science, Institut Teknologi Sepuluh Nopember, Surabaya 60111, Indonesia
[g] Faculty of Civil Engineering, University of Technology Malaysia (UTM), Johor Bahru, 81310 Johor, Malaysia
[h] School of Chemical Sciences, Universiti Sains Malaysia, Penang 11800, Malaysia

ARTICLE INFO

Keywords:
Copper
Ciprofloxacin
Adsorption
Hydroxyapatite
Geopolymer

ABSTRACT

The efficacy of copper Cu(II) adsorption is significantly affected by the presence of antibiotics, such as ciprofloxacin (CIP). Therefore, researchers are highly interested in conducting extensive investigations on the simultaneous adsorption of Cu(II) and CIP. However, most of the adsorbents exhibited low adsorption capacity of CIP with increasing Cu(II) concentration due to the competition for adsorption sites. Hence, the integration of various adsorbents into a single composite could be an effective way to increase the adsorption sites. Thus, this study aims to incorporate hydroxyapatite (Hap) into metakaolin/sludge based geopolymer adsorbent for simultaneous adsorption of Cu(II) and CIP. The effect of different filler loading of Hap (1–3 %) on the metakaolin/sludge geopolymerization and also on the removal efficiency of Cu(II) and CIP were studied in a single and binary system. Moreover, the effects of varied concentrations of Cu(II) (0–100 mg/L) on the removal efficiency of CIP were investigated. Characterization techniques such as x-ray diffraction (XRD), fourier-transform infrared spectrometry (FTIR), scanning electron microscopy (SEM), brunauer-emmett-teller (BET) and neutron tomography imaging were employed to characterize the physicochemical properties of the synthesized geopolymer. It was found that the Hap content has a significant impact on the removal efficiency of CIP and Cu(II). The addition of 2 % Hap providing more nucleation site for the increasing geopolymerization (C-A-S-H) and silicoalumino phosphate gel (SAP) leading to the formation of highly cross-linked geopolymer network and abundant active sites which would favour the adsorption. Moreover, the removal efficiency of CIP by 2 % Hap-geopolymer increased (25.6 % to 61.51 %) with increasing Cu(II) concentration by the complexation and bridging effect between Cu(II) and CIP resulting in the formation of GMK25S1-2Hap-Cu(II)-CIP complexes. Therefore, the hybrid method of geopolymer and Hap is an exceptionally efficient approach for the treatment of wastewater that comprises Cu(II) and CIP.

1. Introduction

As industrialization advances rapidly, significant amount of dangerous, bio-accumulative, and non-degradable heavy metal ions are eventually released into the environment. Copper, Cu(II) is one of the most hazardous metals under the standards set by the US Environmental Protection Agency (Fang Li et al., 2017). For example, the presence of Cu (II) with more than 1.3 mg/L dosage can cause organ damage and lung

* Corresponding author at: Centre of Excellence Geopolymer & Green Technology (CEGeoGTech), Universiti Malaysia Perlis (UniMAP), 01000 Perlis, Malaysia.
E-mail address: mustafa_albakri@unimap.edu.my (M.M.A.B. Abdullah).

https://doi.org/10.1016/j.arabjc.2024.105745
Received 29 January 2024; Accepted 18 March 2024
Available online 21 March 2024

cancer in humans. Cu(II) has also been widely employed as a feed addition in the livestock and poultry industries due to its growth-promoting impact (Wang et al., 2020; Sha et al., 2022; Ling et al., 2019). Furthermore, the presence of ciprofloxacin (CIP) has been consistently detected in wastewater effluent and has recently gained recognition as a prominent emerging environmental contaminant (Hu et al., 2022). It can be discharged into water sources due to inadequate metabolism in humans or from drug manufacturing effluents. CIP concentrations have been detected in water and wastewater at concentrations typically lower than 1 μg/L. However, higher concentrations ranging from 3 to 87 μg/L have been reported in hospital effluents, and drug production facilities has been found to have concentrations as high as 31 mg/L (Hettithanthri et al., 2022). The removal efficiency of Cu(II) is strongly affected by the presence of antibiotics such as CIP as it has a strong affinity to complex with Cu(II) (Yao et al., 2023). The functional group of CIP allows antibiotics to connect with other chemicals, particularly metal ions to form metal-antibiotic complexes. Therefore, the concurrent elimination of antibiotics and heavy metals has garnered increased attention.

Various methods have been employed to remove antibiotics and heavy metals, including advanced oxidation process, membrane separation, ion exchange, chemical precipitation, and adsorption (Jiang et al., 2018; Zhou et al., 2022; Deng et al., 2020). Adsorption is the most advantageous due to its low cost, simple working mode, eco-friendliness, and general applicability for the removal of diverse pollutants (Cao et al., 2022; Xu et al., 2023). During last decade, the number of publications on the co-adsorption of antibiotics and heavy metals has significantly increased, particularly in 2021 and 2022, demonstrating that this topic of research is well-investigated. Simultaneously removing antibiotics and heavy metals poses a greater challenge compared to removing single pollutants due to factors namely (i) competition for the adsorption site, (ii) significant complexation of solutes, or (iii) development of ternary surface complexes. Different solids are considered as sorbents for this purpose, including activated carbon, biochar, resin, silica, clay, zeolite, geopolymer and hydroxyapatite. However, the majority of samples exhibited a decrease in their capacity to adsorb CIP with increasing concentration of Cu(II) which can be attributed to the competition for available adsorption sites. In a recent study conducted by, Lv et al. (Lv et al., 2023), reported the low concentration of Cu(II) (0–20 mg/L), promoted the CIP adsorption on adsorbents. However, a higher concentration of Cu(II) (100 mg/L) hindered the adsorption capacity of CIP due to the saturation of active sites, resulting in a competitive interaction between Cu(II) and CIP. Hence, the careful selection of the adsorbent holds significant importance.

Hydroxyapatite (Hap) is a cheap, stable, and sparingly soluble salt that can be made by precipitating calcium phosphate solution (Bazargan-Lari et al., 2011). Hap is a biomaterial and inorganic substance, is being extensively researched for various kinds of wastewater treatment applications (Pooladi and Bazargan-Lari, 2020, 2023). In addition, Hap exhibits potential physicochemical properties, including robust chemical stability, non-toxicity, exceedingly low solubility, porous structure, and remarkable adsorption capacity (Jia et al., 2023; Bazargan-Lari et al., 2014). The following are some examples of potential reaction mechanisms for metal immobilisation in Hap: (a) ion exchange processes, (b) surface complexation, (c) Hap dissolution and precipitation of new metal phosphates, and (d) substitution of calcium in Hap by other metals during re-crystallization (co-precipitation) (Bazargan-Lari et al., 2011). Hap has been reported to remove certain heavy metal ions, including those of copper, zinc, cobalt, cadmium, and lead (Bambaeero and Bazargan-Lari, 2021). Moreover, due to the presence of two different types of charged active sites on its surface, namely cationic Ca^{2+} and PO_4^{3-} anionic sites, studies have shown that Hap exhibits exceptional adsorption capacity for certain antibiotics (Laabd et al., 2021). Recently, Pooladi et al. (Pooladi and Bazargan-Lari, 2023) developed a low cost natural composite made of snail shell, hydroxyapatite and chitosan for the simultaneous removal of copper and zinc. However, there is no documented literature on the simultaneous removal of heavy metal and antibiotic by using Hap, although it exhibited significant adsorption of ciprofloxacin, tetracycline (TC), and chlortetracycline.

On the other hand, geopolymers, or inorganic polymers, have gained increasing interest in recent years for purifying aqueous media due to their unique and diverse physicochemical properties, such as their porous nature, large adsorption capacity by ion exchange, physical-thermal stability, low-cost, and availability of feedstocks (Ge et al., 2015; Petlitckaia et al., 2020). In addition, the chemical structure of geopolymer with a negatively charged aluminosilicate framework balanced by cations (Na^+, K^+, or Cs^+) can be exchanged with cations in the solution. As a result, this characteristic serves as a basis for the removal of heavy metal ions from wastewater. Therefore, combining Hap and geopolymer could be an effective way to combine the advantages of both adsorbents into a single composite adsorbent that could remove a variety of contaminants. This composite material demonstrates high pollutant removal capability, ultimately producing multi-functional adsorbents by merging the unique mechanisms of several adsorbents. However, to the best of our knowledge, there has not been any published research on the simultaneous adsorption of antibiotics and heavy metals using Geopolymer/Hap. Thus, this study aimed to develop and characterize Hap incorporated geopolymer adsorbent and to explore the removal behaviour of CIP and Cu(II) in a single and binary systems.

The main objectives of this research were: (1) to investigate the effect of addition of Hap at different filler loading on the geopolymerization and also on the removal efficiency of Cu(II) and CIP in a single and binary system; (2) to explore the impact of Cu(II) concentration on the effectiveness of CIP removal; (3) to explain the interaction mechanism of Cu(II) and CIP by synthesized geopolymer by means of characterization.

2. Materials

The raw materials used in this study were metakaolin (MK), sludge type 1 (S1), and synthesized Hap. While the chemicals used in this study were ciprofloxacin ($C_{17}H_{18}FN_3O_3$), copper sulphate pentahydrate ($CuSO_4 0{\cdot}5H_2O$), sodium silicate (Na_2SiO_3), sodium hydroxide (NaOH), hydrochloride acid (HCl) and diammonium phosphate $(NH_4)_2HPO_4$. The ciprofloxacin, with a molecular weight of 331.34 g/mol was purchased from MedChemExpress. In addition, NaOH and Na_2SiO_3 were provided by Formosa Plastic Corporation, Taiwan, and South Pacific Chemical Industries Sdn Bhd, Perai, Penang, Malaysia, respectively, while HCl was supplied by Sigma Aldrich. NaOH and Na_2SiO_3 were used to prepare an alkaline activator solution.

2.1. Methods

2.1.1. Preparation of Metakaolin/Sludge incorporated with hydroxyapatite based geopolymer adsorbent

In the preparation of geopolymer, MK and S1 were used as aluminosilicate sources, and the preparation steps of these aluminosilicate precursors, including their chemical composition, have been provided in our previous work (Arokiasamy et al., 2022). In our previous work, the geopolymer adsorbents prepared at 25 % of MK and 75 % S1 (GMK25S1) at S:L ratio of 0.6, was considered as the best ratio for an effective adsorbent among various compositions based on the workability and the removal efficiency of Cu(II). In the current study, the synthesized Hap was added as an additional material in the geopolymerization process to the total weight of the geopolymer to increase the adsorption sites for simultaneously removing Cu(II) and CIP. First, the solid precursors (MK, S1, and Hap) and liquid precursors (Na_2SiO_3 and NaOH) were weighed according to Table 1, which was calculated according to different filler loadings of Hap (1–3 wt%). A varied filler loading of Hap (1–3 %) was selected based on the workability of MK/sludge-based geopolymer paste at a S:L ratio of 0.6. Since the workability of MK/sludge-based

Table 1
Weight mass ratio of solid and liquid precursors for geopolymerization.

Sample	Metakaolin (g)	Sludge 1 (g)	Na_2SiO_3 (g)	NaOH (g)	Hydroxyapatite (g)
GMK25S1					–
GMK25S1-1Hap					2.7 (1 %)
GMK25S1-2Hap					5.3 (2 %)
GMK25S1-3Hap					8.0 (3 %)

geopolymer paste is lowest at > 3 % of Hap caused by the reduced fluidity due to less water and more powder, the loading below 3 % is taken into consideration for the geopolymerization process. Next, the solid precursors were mixed well to obtain homogeneity before mixing with liquid precursors. After that, the solid precursors were mixed with an alkaline activator (Na_2SiO_3: 10 M NaOH = 1.5) at predetermined solid-to-liquid (S: L = 0.6) by using a mechanical mixer for 15 mins. After mixing, the obtained geopolymer paste was cured in an oven at 60 °C for 2 days. After that, the hardened geopolymer was crushed into powder particles and sieved through 300 μm to obtain uniform particle size distribution. The formulated products were labelled GMK25S1-1Hap, where 1Hap represents filler loading of Hap, MK25S1 represents 25 % of MK and 75 % of S1, and G represents the geopolymerization process.

2.1.2. Batch adsorption experiment of copper ions and ciprofloxacin

Several batch adsorption tests were carried out to investigate the ability of Hap incorporated GMK25S1 geopolymer adsorbent to remove Cu(II) and CIP. In order to conduct the adsorption process, the stock solution of Cu(II) and CIP was prepared. The stock solution of Cu(II) was prepared by dissolving 3.93 g of copper sulphate pentahydrate ($CuSO_40{\cdot}.5H_2O$) in distilled water. At the same time, the stock solution of CIP was prepared by dissolving 1 g of CIP in 1L of 0.1 N HCl. Then, the stock solution of Cu(II) and CIP was diluted into 100 mg/L and 40 mg/L, respectively, for further use. The adsorption test of CIP and Cu^{2+} was conducted in a single and binary system. Thus, the adsorption parameters, such as initial metal concentration, adsorbent dosage, pH, and contact time, were kept constant as tabulated in Table 2 to distinguish the interaction between CIP and Cu^{2+} in single and binary systems at fixed conditions.

Based on the literature, the adsorption of Cu^{2+} in single system without CIP was comparable to the simultaneous adsorption of Cu^{2+} and CIP in binary system (Le et al., 2024; Li et al., 2017). However, in comparison to CIP alone, the adsorption of CIP in binary system with the coexistence of Cu^{2+} was increased considerably. This behaviour can be explained by the development of the Cu^{2+}-CIP complex. As Cu(II) had a substantial impact on CIP adsorption, the adsorption parameters of Cu (II) were therefore considered to be the ideal conditions for the simultaneous adsorption of Cu(II) and CIP. According to our earlier research on the adsorption of Cu^{2+} by MK/S1-based geopolymer (Arokiasamy et al., 2022), the optimum parameters for Cu^{2+} adsorption were an initial concentration (100 mg/L), time (60 min), pH (7) and adsorbent dosage (0.15 g). Furthermore, the initial concentration of CIP was fixed at 40 mg/L for the simultaneous adsorption of Cu(II)/CIP in this work, considering the highest concentration of CIP on wastewater. However, pH is the critical factor in the complex formation and heavy metal speciation during the simultaneous adsorption of Cu^{2+} and CIP in binary system. Despite, the largest component of $[Cu\text{-}CIP]^{2+}$ complex was observed in the pH range of 5.0–7.0 and the adsorption of Cu^{2+} and CIP was simultaneously promoted at pH 7 (Ma et al., 2020). However, at pH > 8, Cu^{2+} precipitate and bind with hydroxide ions and hindered the adsorption process. Moreover, zwitterionic $CIP^{\pm}$ is the most reactive form of CIP (Laabd et al., 2021). Thus, pH 7 was selected and maintained constant for each batch adsorption experiment., where the Cu^{2+} ions were added into the synthetic water containing CIP at pH 7, reflecting the real wastewater system at which Cu^{2+} preequilibrated with CIP, and most of the Cu^{2+} ions formed complexes with CIP.

Table 2
Adsorption parameters of CIP and Cu^{2+}.

Adsorption parameter	CIP	Cu^{2+}
Initial concentration (mg/L)	40	100
Dosage (mg)	0.15	0.15
pH	7	7
Time (h)	1	1

However, a previous study by Zhao et al. (Zhao et al., 2022) on the effect of Cu(II) concentration (0–100 mg/L) on the removal effectiveness of CIP reported that the removal capacity of CIP improved under coexistence of low Cu(II) concentration (1–15 mg/L) and then reduced with the continuos adding of CIP. Additionally, Lv et al. (Lv et al., 2023) previously reported that a low concentration of Cu(II) (0–20 mg/L) promoted the adsorption of CIP on polyethylene microplastics. While, higher concentration of Cu^{2+} (100 mg/L) hindered the adsorption capacity of CIP due to the saturation of active sites. Thus, the effect varied concentration of Cu^{2+} on the removal efficiency of CIP was set in the range between (0–100 mg/L) to validate the availability of adsorption sites resulting from the incorporation of Hap into GMK25S1. Consequently, an aqueous solution (100 mL) containing 50 mL of Cu(II) and 50 mL CIP was introduced along with the 0.15 g of Hap incorporated GMK25S1 geopolymer adsorbent into the conical flask, and the pH of the solution was adjusted to pH 7 by using 0.1 M HCI and 0.1 M NaOH. Then, the mixture was shaken vigorously on an orbital shaker at 220 rpm. After 1 h, the resultant solution was filtered through Whatman filter paper grade 93, 12.5 cm before being filtered through 0.45-μm membranes. Following filtering, the samples were subjected to Atomic absorption spectroscopy (AAS) and Ultraviolet–visible spectroscopy (UV–vis) analysis, respectively, and the removal efficiency, R (%), and adsorption quantity (q_{max}) of Cu^{2+} and CIP were then calculated using Eqs. (1) and (2), respectively.

$$R(\%) = \frac{Ci - Ct}{Ci} \times 100 \tag{1}$$

$$q_{max}\left(\frac{mg}{g}\right) = \frac{(Ci - Ct)}{m} \times v \tag{2}$$

Where, Ci (mg/L) and Ct (mg/L) were initial concentration and final concentration at time of Cu(II) and CIP respectively, V (L) is the volume of the solution and m (g) is the mass of the geopolymer adsorbent.

2.1.3. Characterization and testing

Various characterization techniques were used to explore the physiochemical properties of Hap incorporated GMK25S1 geopolymer adsorbent. The effect of Hap addition on the phase stability of geopolymer was analysed by conducting X-ray diffraction (XRD) (model Bruker D2 Phaser), using Cu-Kα (at wavelength 1.54184 [A]) radiation, fitted with a Cu tube on the secondary optics, and scanned in the range between 5 and 70°. The surface functional groups of the Hap incorporated geopolymer were characterised by Fourier-transform infrared spectroscopy (FTIR) using PerkinElmer (Frontier) to record transmittance spectra in the 450–4000 cm^{-1} region, with a resolution of 4 cm^{-1} (8 scans). In contrast, the effect of Hap addition on the surface morphology of geopolymer were observed by scanning electron microscopy (SEM) JEOL JSM-6460LA which can produce images up to 10,000 magnifications. Additionally, the distribution of porosity saturated

water in geopolymer paste was observed from the neutron tomography images obtained at Imaging and Materials Science & Engineering (IMAT) beamline, ISIS Neutron and Muon Source, Rutherford Appleton Laboratory, United Kingdom. The IMAT tomography camera was equipped with a 2048 × 2048-pixel Andor Zyla sCMOS 4.2 PLUS. The camera pixel size was 31 μm. The samples were stacked inside an aluminium tube fastened to the rotating platform and placed 10 m from the neutron beam and 25 mm from the pixel detector. A total of 396 projections were collected, each with a 30 s exposure time, for a total scan time per tomogram of almost 6 h. Several open-beam and dark images were gathered for flat fielding before and after every tomography scan. Moreover, the surface area and pore characteristics of the sample were measured by a N_2 adsorption–desorption technique using the Brunauer–Emmett–Teller (BET) and Barrett–Joyner–Halenda (BJH) models. The samples were degassed at room temperature for 24 h. Then, the adsorption–desorption temperature was 77 K, using N2 as an adsorptive gas molecule in a (Micromeritics Tristar II). Besides, XRD, FTIR and EDS (energy-dispersive x-ray spectroscopy) were performed on the adsorbed Cu(II)/CIP-geopolymer adsorbent to illustrate the adsorption mechanism.

On the other hand, analytical testing such as AAS and UV–vis were conducted to measure the residual concentration of Cu(II) and CIP, respectively. After the batch adsorption of Cu(II), the supernatant liquid of the reaction was filtered through Whatman Grade 93, 12.5 cm diameter filter paper and then 50 mL of the solution was separated in a container. The changes in the Cu(II) concentration before and after adsorption was determined by conducting AAS (model Perkin Elmer Analyst 800). After the batch adsorption of CIP, the resultant solution was filtered by using a membrane syringe filter, polyvinylidene fluoride (PVDF) 0.45 μm, 25 mm diameter. An aliquot of the solution was separated in a container after filtration. Then, the sample was placed in quartz cuvette and the transmitted light in UV–Vis (model Perkin Elmer Lambda 365) at a wavelength of 268 nm was measured to determine the changes in the concentration of CIP before and after adsorption.

3. Results and discussion

3.1. Removal efficiency of Cu(II) and CIP in a single and binary system

The batch adsorption experiment was conducted to elucidate the removal efficiency of Cu(II) and CIP in a single and binary system. The removal efficiency of Cu(II) and CIP by GMK25S1 with and without the addition of Hap in a single system is presented in Fig. 1. The adsorption efficiency of GMK25S1 for CIP was low in the absence of Hap supplementation. However, the addition of Hap in the geopolymerization resulted in a significant enhancement in the adsorption performance of GMK25S1 for CIP. In a single system, the removal efficiency of CIP by GMK25S1 increases with increasing Hap amount and achieves the highest removal efficiency of CIP (25.6 %) for GMK25S1-2Hap as shown in Fig. 1(a). The aforementioned behaviour may be associated with the presence of Ca^{2+} in Hap, which can react with alumina-oxygen tetrahedra $[AlO_4]^-$ and silica-oxygen tetrahedra $[SiO_4]^-$ dissolved in MK and S1 to generate amorphous calcium aluminium silicate hydrate (CASH) gel. Moreover, the presence of Ca^{2+} in the reaction system can behave as nucleation sites which can promote dissolution of silicon (Si) and aluminium (Al) in MK and S1 contributing to the formation of greater content of geopolymer gel phases. Besides, the crystalline phases such as berlinite ($AlPO_4$), akermanite ($Ca_2MgSi_2O_7$) and calcite ($CaCO_3$) were developed by the incorporation of Hap. In addition, the incorporation of Hap in the geopolymerization increases the number of functional moieties such as AlO^-, SiO^-, PO^-, CO_3^{2-} and cations such as Ca^{2+} and Mg^{2+} that are exposed for CIP adsorption. The molecular structure of CIP contains two ionizable groups: the secondary amino group (HN_3^+) of the piperazine ring linked to C7 and the C3-carboxylic group ($-COO^-$). At the same time, the prepared GMK25S1-2Hap become deprotonated at pH 7 and carries negative charges as expressed in Eqs. (3)–(5). Thus, CIP adsorption was more favorable at pH 7, where $\equiv PO^-$, (Al or Si)-O^- and CO_3^{2-} groups were predominant and tend to be electrostatically attracted by HN_3^+ during CIP adsorption. Meanwhile, the positively charged Ca^{2+} and Mg^{2+} ions could form complexes with $-COO^-$ groups of $CIP^{\pm}$ as listed in Eqs. (6)–(9). Therefore, the introduction of Hap demonstrated a notable enhancement in the adsorption capabilities, further validating the superior efficacy of the functionalized GMK25S1-2Hap in removing hazardous antibiotics from aqueous solutions. Thus, the Hap adsorption sites in the resulting GMK25S1-2Hap adsorbents were primarily responsible for the increase in the removal effectiveness of CIP. This demonstrates the advantageous synergy between geopolymer and Hap for enhancing the CIP removal effectiveness of the adsorbents. However, the removal efficiency of CIP was declined with the incorporation of 3 % of Hap in the geopolymerization process. This results from having an excessive Hap particle, which destroys the geopolymer structure and induce steric hindrance.

Moreover, the removal efficiency of Cu(II) by GMK25S1 is slightly increased from 99 % to 99.9 % after the incorporation of Hap. It maintained the maximum level of removal efficiency, indicating that the addition of Hap had no adverse effect on the removal efficiency of Cu(II) as can be observed from Fig. 1(b). Cu(II) is entirely soluble up to a pH of 6.0, after which it gradually binds to OH– and precipitates as $Cu(OH)_2$. As long as the adsorbent surface is negatively charged, hydrated Cu(II) with a positive charge is predominantly adsorbed via electrostatic

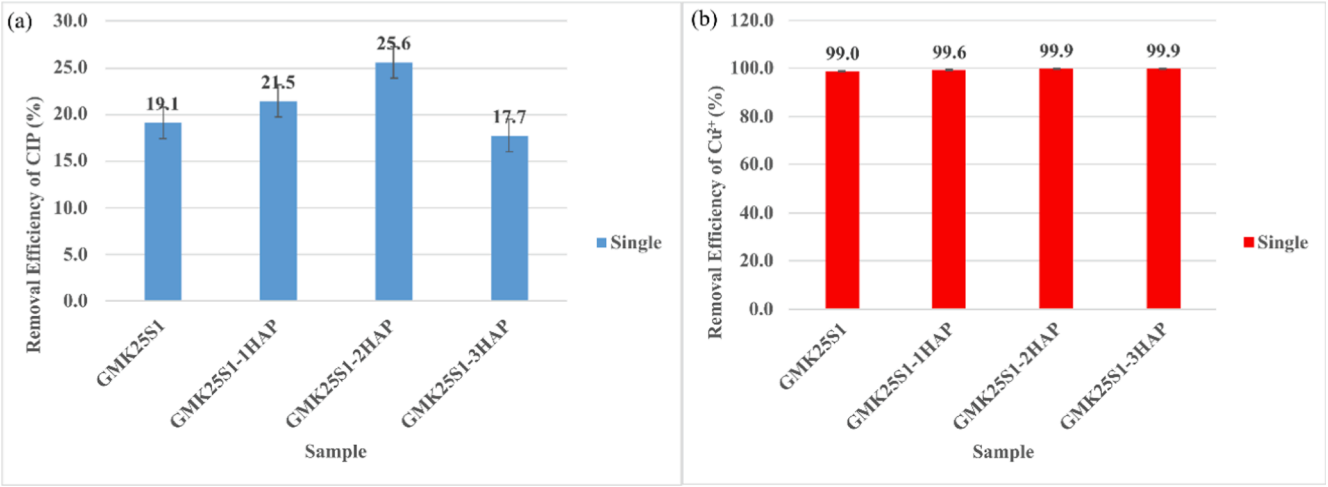

Fig. 1. Removal efficiency of (a) CIP and (b) Cu(II) in a single system.

attraction and ion exchange with cations such as Ca^{2+} and Mg^{2+} in GMK25S1-2Hap. In addition, Cu(II) penetration into the additional mesopores formed in geopolymer with increasing CASH gel, was favored due to its small ionic radius.

Deprotonation of GMK25S1-2Hap

$$\equiv (AlorSi) - OH_2{}^{+} \overset{-H^+}{\leftrightarrow} \equiv (AlorSi) - OH \overset{-H^+}{\leftrightarrow} \equiv (AlorSi) - O^- \quad (3)$$

$$\equiv P - OH \overset{-H^+}{\leftrightarrow} \equiv PO^- \quad (4)$$

$$\equiv HCO_3{}^{-} \overset{-H^+}{\longleftrightarrow} \equiv CO_3{}^{2-} \quad (5)$$

Complexation

$$\equiv (AlorSi) - O^- + HN_3{}^{+} \rightarrow [Attraction] \quad (6)$$

$$\equiv PO^- + HN_3{}^{+} \rightarrow [Attraction] \quad (7)$$

$$\equiv CO_3{}^{2-} + HN_3{}^{+} \rightarrow [Attraction] \quad (8)$$

$$\equiv Ca^{2+} or Mg^{2+} + COO^- \rightarrow [Complexation] \quad (9)$$

On the other hand, Fig. 2 presents the removal efficiency of CIP and Cu (II) in a binary system with and without the addition of Hap. In a binary system, the removal efficiency of CIP was significantly increased with the coexistence of Cu(II) and GMK25S1-2Hap obtained the highest removal efficiency of CIP (61.5 %), as shown in Fig. 2(a). Based on Fig. 2 (b), the removal efficiency of Cu(II) by the synthesized GMK25S1-2Hap adsorbent in the presence of CIP was slightly reduced from 99.9 to 96.62 % in comparison with the single system. Similar finding was obtained by Feng et al. (Feng et al., 2022), which highlighting a reduction in the Cu (II) adsorption in binary system with the coexistence of TC caused by the strong coordination between Cu(II) and TC reduces its interaction with the functional groups in the sorbent, and the creation of TC-Cu(II) complex changes the surface charge and molecular size of Cu(II). However, it maintained the high removal efficiency of Cu(II) greater than 90 %, indicating that the adsorption of CIP and Cu(II) were mutually promoted over the GMK25S1-2Hap.

The conjugated aromatic rings in the CIP molecule have a high electron density in general. In contrast, the uppermost layer of the Cu(II) nucleus has six unoccupied orbitals that can accept lone pairs of electrons (Sha et al., 2022). As a result, complexation between CIP and Cu (II) is likely to occur, and this complexation might then operate as a bridge to boost their adsorption over GMK25S1-2Hap at the same time. Thus, cation bridging and complexation are believed to be the primary mechanisms for the simultaneous adsorption of CIP and Cu(II) as shown in Eqs. (10)–(14). The adsorption of Cu(II) on adsorbent surfaces that carry a negative charge can serve as supplementary active sites. These active sites can then form complex structures with –COO^- of CIP, resulting in the formation of a ternary complexation (GMK25S1-2Hap-Cu(II)-CIP) as expressed in Eq. (13). At the same time, additional CIP and Cu(II) can also combine to form a quaternary system, as illustrated in Fig. 3. Therefore, the improvement of CIP adsorption is contingent upon the metal cation's ability to coordinate. According to the Irving-William series, the Cu(II) complexes are very stable, showing that Cu(II) is an excellent central atom for CIP (Ma et al., 2020). Additionally, whether metals can cause high-strength coordination between them depends on the properties and structural characteristics of whether they can act as "mediators" in antibiotic adsorption to aid synergistic elimination. In accordance with the Hard-Soft-Acid-Base theory (HSAB), CIP are soft bases and frequently combine with soft acids. Cu(II) is considered borderline acid, and it possesses low chemical hardness (Wang and X. yi You, 2023). Hence, Cu(II) is more likely to bind with soft bases. Moreover, the smaller the radius of Cu(II), the higher the ionic charge and the easier it is to develop stable complexes. Thus, Cu(II) could function as a mediator in a binary system to encourage the synergistic elimination based on the close coordination between Cu(II) and CIP.

Complexation

$$Cu^{2+} + GMK25S1 - 2Hap^{-} \leftrightarrow [GMK25S1 - 2HaP - Cu]^{2+} \quad (10)$$

$$HN_3{}^{+} + GMK25S1 - 2Hap^{-} \leftrightarrow [GMK25S1 - 2HaP - HN_3] \quad (11)$$

$$COO^- + [Cu^{2+}] \leftrightarrow [Cu - COO]^{2+} \quad (12)$$

Cation bridging

$$COO^- + [GMK25S1 - 2Hap - Cu]^{2+} \rightarrow [GMK25S1 - 2Hap - \mathbf{Cu} - COO]^{2+} \quad (13)$$

$$[Cu - COO]^{2+} + GMK25S1 - 2Hap^{-} \leftrightarrow [GMK25S1 - 2HaP - \mathbf{Cu} - COO]^{2+} \quad (14)$$

3.2. Effect of Cu^{2+} concentration on the removal efficiency of CIP

Moreover, the effect of Cu(II) ion concentration on the removal efficiency of CIP is presented in Fig. 4(a). At a low concentration of Cu(II) (20 mg/L), the removal efficiency of CIP was slightly promoted (45.43 %) due to the competition for same adsorption sites. While, the increase in Cu(II) concentration (20–100 mg/L) strengthens the promotion effect (45.43 % to 61.51 %). It was hypothesized that the complexation-bridging between Cu(II) and CIP on the adsorbent increased the amount of CIP that was adsorbed, as shown in Fig. 4(b). Besides, in binary system, the percentage of $[Cu(II)\text{-}CIP]^{2+}$ greatly increased, as Cu^{2+}

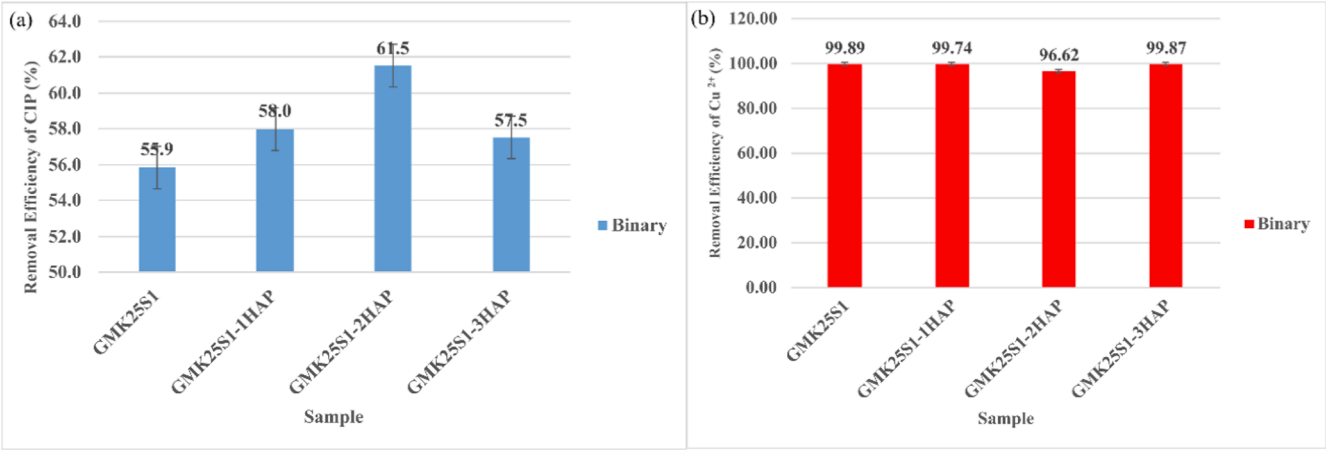

Fig. 2. Removal efficiency of (a) CIP and (b) Cu(II) in binary system.

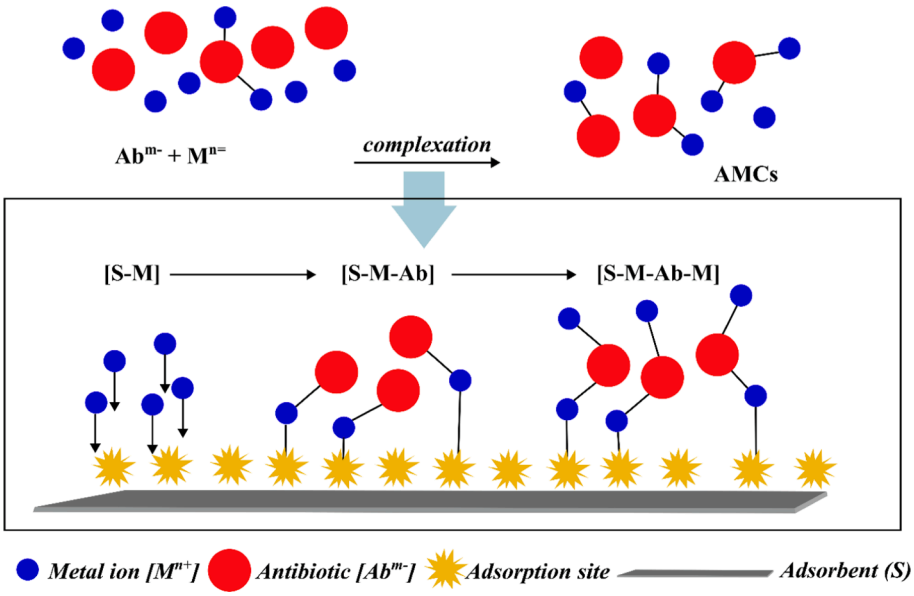

Fig. 3. Formation of ternary and quaternary complexes (Khurana et al., 2021).

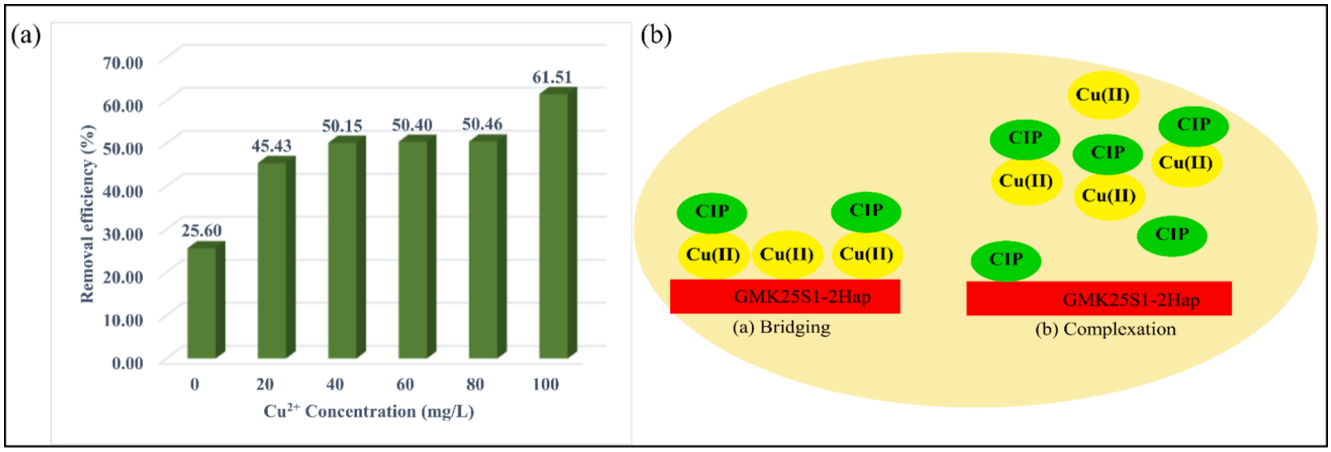

Fig. 4. (a) Effect of Cu^{2+} concentration on CIP removal efficiency and (b) complexation mechanism.

preequilibrated with CIP and became the dominant species in the binary system. The electrostatic interaction between $[Cu(II)\text{-}CIP]^{2+}$ with the negatively charged GMK25S1-2Hap surfaces increased the uptake of CIP due to high positive surface charge compared to CIP^0 and CIP^+. Moreover, as the concentration of Cu(II) increased, more Cu(II) ions were produced, causing a change in the packing, spacing, or alignment of adsorbed CIP (Fang Li et al., 2017). This can be explained by the interaction between Cu(II) and GMK25S1-2Hap which neutralized repulsive forces between GMK25S1-2Hap and $–COO^-$ group of CIP, thus creating favourable sorption sites. Thus, based on the aforementioned hypothesis, it can be inferred that the GMK25S1-2Hap synthesized in this research exhibits a substantial number of active sites capable of facilitating CIP with increasing Cu(II) concentration.

3.3. Characterization on hydroxyapatite incorporated Metakaolin/ Sludge-Based geopolymer adsorbent

3.3.1. Phase analysis

Fig. 5 displays the XRD pattern of Hap incorporated GMK25S1 with Hap contents of 1, 2 and 3 %. It is evident that the dominant mineral phases in GMK25S1 geopolymer were identified as quartz (SiO_2), albite ($NaAlSi_3O_8$) and hematite (Fe_3O_4). The presence of albite suggests that sodium aluminium silicate hydrate (NASH) gel is forming in the GMK25S1 geopolymer. In addition, there was a significant decrease in the intensity peak of quartz at $2\theta = 26.5°$ indicating that Hap improve the reaction degree of precursors thereby consuming quartz in MK and S1 which was similar with the findings of Yang et al. (Yang et al., 2024). In contrast, anorthite ($CaAlSi_2Si_2O_8$), berlinite, akermanite and calicte was found to be the predominant mineral phase in Hap incorporated geopolymers. Anorthite reflecting the formation of CASH gel in Hap incorporated GMK25S1. Moreover, the broad bumps in the Hap incorporated GMK25S1 geopolymer expanded to the right and their areas increased in comparison to the GMK25S1, suggesting that the addition of Hap caused the production of CASH gels and that the amount of gels geopolymers increased as the Hap content increased.

Moreover, the central positions of the broad diffraction pattern in all the samples are approximately at 27° (2θ). This finding is consistent with silico-aluminophosphate (SAP) geopolymerization, as demonstrated by earlier research Louati et al. (Louati et al., 2016), where a broad diffraction pattern centred at 27° (2θ) were identified as amorphous hydrated berlinite. Berlinite is the only known mineral that is isostructural with quartz. Berlinite can have the same structure as quartz as the Al-O and P-O have bond lengths of 1.73 Å and 1.63 Å respectively, similar in size to Si-O (1.63 Å) (Joseph, 2008). Thus, the same structure

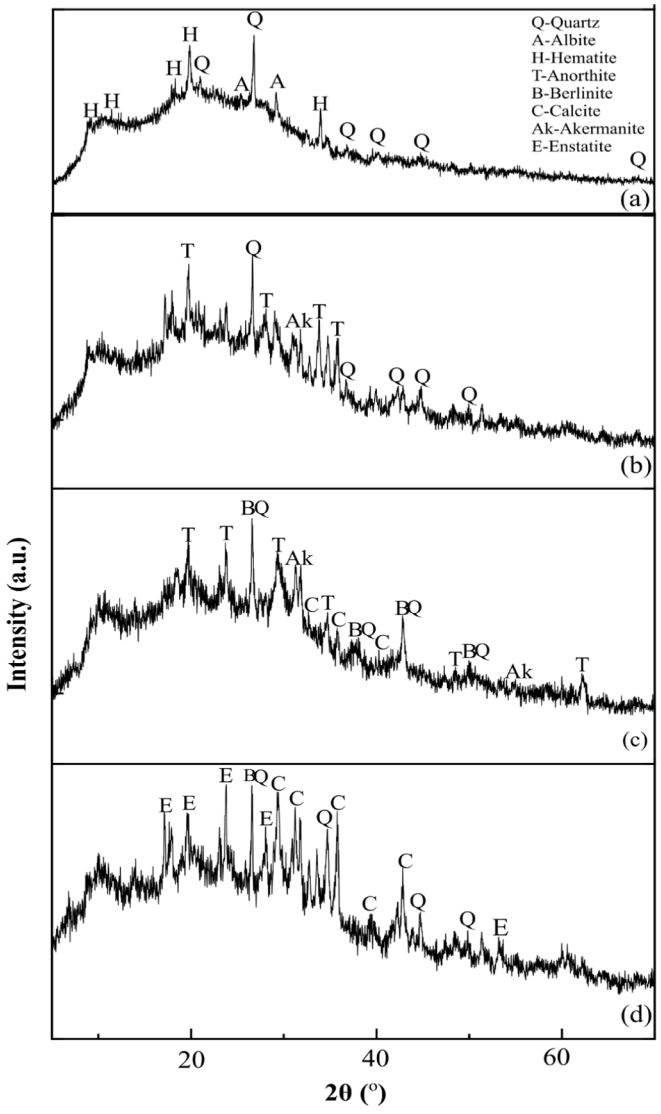

Fig. 5. XRD pattern of geopolymer (a) GMK2S1, (b) GMK25S1-1Hap, (c) GMK25S1-2Hap and (d) GMK25S1-3Hap.

can be created when the phosphorus (P) and aluminium (Al) completely replace the silicate (Si) without changing the quartz structure. According to Wagh et al. (Wagh, 2016), the crystalline compound formation of berlinite develop very quickly during geopolymerization, even at room temperature. The phosphorus oxygen tetrahedron $[PO4]^{+}$ is positively monovalent when it enters the network structure of geopolymers, which can balance the negative charge of aluminium oxygen tetrahedron $[AlO_4]^{-}$ and cations are not required for charge balance ensuring the stability of the SAP geopolymer structure. On the other hand, the Al or Si in its network structure is partially or completely replaced by P, and the basic unit SAP geopolymer are -Si-O-Al-O-P-, -Si-O-P-O-Al- or -Al-O-P-. Thus, the network gel of Hap incorporated GMK25S1 is identified as the combination of SAP and CASH gel.

In addition, after geopolymerization, new peak related to calcite phase was observed in GMK25S1 incorporated Hap due to the carbonation. Calcite is formed by the reaction between the residual $Ca(OH)_2$ in the synthesized Hap with diffused atmospheric carbonate. However, the intensity of this peak became more prominent in GMK25S1-3Hap due to increase in the unreacted Hap particles caused by the low degree of geopolymerization when the Hap filler loading is more than the optimum amount. Calcite in GMK25S1-3Hap shows no new phase, and the presence of characteristic rays of calcite in the geopolymer containing calcium carbonate indicates that calcite did not react during the geopolymerization. The contribution of calcite to the polymerization mechanism is very low since it is hard to dissolve in a strong alkaline environment. Moreover, the peak intensity of berlinite diminished with increasing Hap content more than 3 % due to the limited availability of Al to react with PO_4^{3-}.

3.3.2. *Functional group analysis*

The FTIR spectra of GMK25S1 with different Hap content is presented in Fig. 6. It was discovered that the FTIR spectra of Hap incorporated GMK25S1 is varied with varying Hap percentages. The broad absorption band at 3440–3470 and 1630–1690 cm^{-1} are attributed for stretching vibration of O-H bond and bending vibration of H-O-H bond, respectively indicating the existence of structural water and free water on the surface geopolymer and their pores. In addition, the bands in the range of 1440–1490 cm^{-1} and 750–758 cm^{-1} was assigned to carbonate (CO_3^{2-}) and stretching vibration of Si-O-Si, respectively. While, the absorption band at 1029 cm^{-1} in GMK25S1 is related to the stretching vibration of Si–O-T (T = Si or Al), which is assigned as a characteristic band of the NASH aluminosilicate gels. With the addition of Hap, the Ca content is increased in the reaction system and C-A-S-H gel was developed as the Ca^{2+} combined with silica-oxygen tetrahedron and alumina-oxygen tetrahedron. Thus, in the Hap incorporated GMK25S1, this peak reflecting the asymmetrical stretching of Si-O-T bonds (T = Si, Al and P).

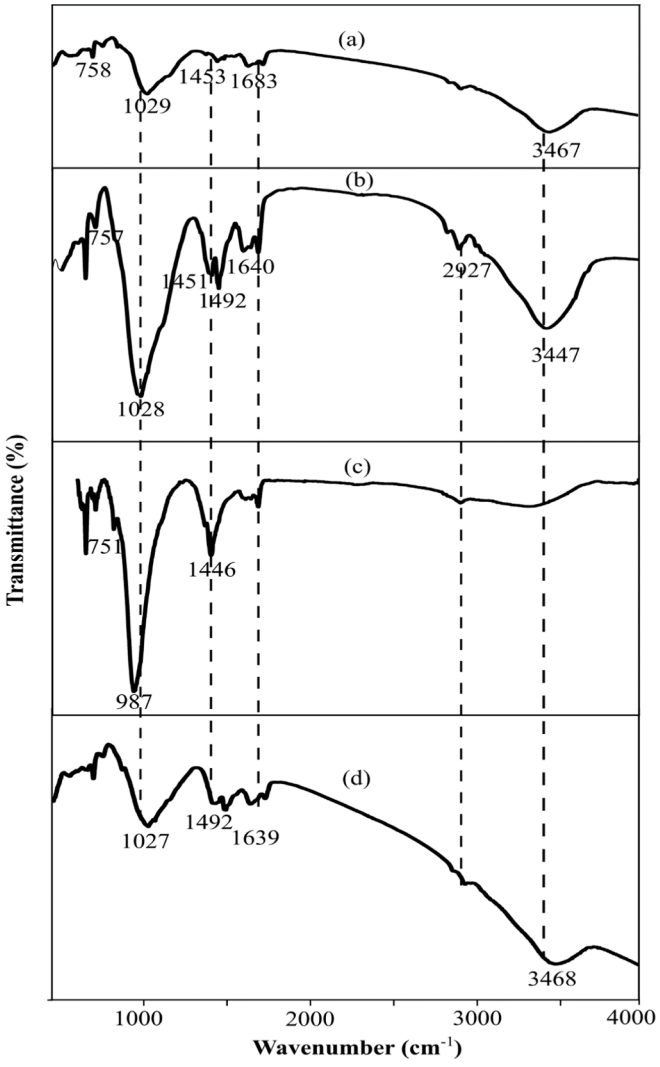

Fig. 6. FTIR spectra geopolymer (a) GMK25S1, (b) GMK25S1-1Hap, (c) GMK25S1-2Hap and (d) GMK25S1-3Hap.

It is challenging to identify the vibration band of the bonds from the phosphate binder (P-O) since the primary band (Si-O-Al) of the CASH aluminosilicate gel in Hap incorporated GMK25S1 overlaps with the central band of the phosphate geopolymer.

However, the absorption peaks of GMK25S1-2Hap were more significant than other samples, these differences suggested a stronger geopolymerization of GMK25S1-2Hap. There has been some specific shift observed towards lower frequency of the bands after the geopolymerization reaction with the incorporation of 2 % of Hap. The major difference was observed for the main characteristic band Si-O-T which differs drastically in position and intensity with the increase of Hap addition. With an increase in the Hap up to 2 %, this band shifted to lower wavenumber (987 cm^{-1}) compared GMK25S1. This fact clearly indicates the effect of Hap on the geopolymerization reaction, in addition to providing more nucleation site for the increasing geopolymerization (C-A-S-H) leading to the formation highly cross-linked geopolymer network. Therefore, it becomes very sharp and more intense which explains that the presence of Hap is favorable for gel formation in geopolymer. Moreover, the band at 987 cm^{-1} of GMK25S1-2Hap are relevant to the existence of Si-O-P-O-Si and Si-O-P units. This results are supported by previous investigation in a study by Pu et al. (Pu et al., 2024), which highlights that the band belong to the Si-O-P stretching vibration occurred in the range of 933–1335 cm^{-1}. Moreover, the absorption band at 757 cm^{-1} was displaced to lower wavenumber 751 cm^{-1} indicating PO_4^{3-} took place in the geopolymerization, so the Si-O-Si unit in S1 changed into Si-O-P-O and Si-O-P units. In addition, identified structures like –Si–O–P–bonds in the geopolymer are easily dissolved in water and form silanol (Si–OH) and P–OH groups,

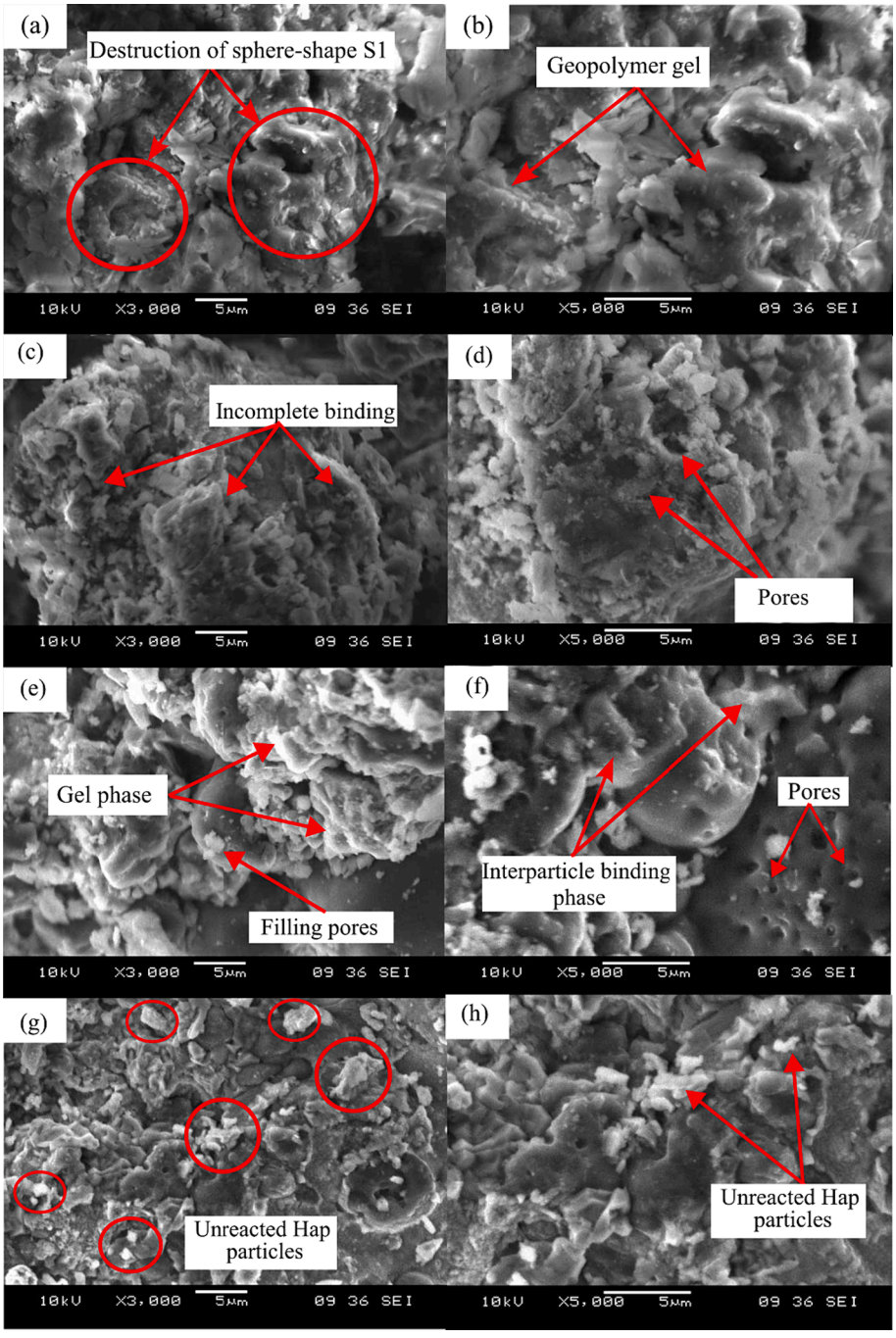

Fig. 7. SEM morphology of geopolymer (a-b) GMK25S1, (c-d) GMK25S1-1Hap, (e-f) GMK25S1-2Hap and (g-h) GMK25S1-3Hap.

which led to the enhanced adsorption properties of geopolymer samples (Ma et al., 2022). Furthermore, at 2 % of Hap, the intensity of band corresponding to the stretching vibration of O-H bond and bending vibration of H-O-H bond decreased gradually demonstrating that the free water decreased, which may be related to the consumption of water in the reaction system during the formation of C-A-S-H. On contrast, the band related to carbonates displaced from 1492 and 1451 cm^{-1} to 1446 cm^{-1} with increasing the geopolymer phases formation results in the reduction of Ca rich phases that are gluttonous for carbonation. Hence, the formation of 3D network structure and increase in the active sites such as (Si-OH, Al-OH, P-OH and HCO_3^-) by the enhanced geopolymerization with increase in the Hap content would favour the adsorption.

On the other hand, the excess PO_4^{3-} results from the further addition of Hap causes charge imbalance and destroy the geopolymer structure. When the percentage of addition is more than 2 % of Hap, the band intensity becomes very weak and it shift to the higher wavenumber explaining the incomplete geopolymerization reaction. In addition, the band formed at 1639 cm^{-1} was attributed to the adsorbed water and the stretching and bending vibration of P–O group indicating the presence excess PO_4^{3-} consistent with previous researches conducted by Allaoui et al. (Allaoui et al., 2023) and Pu et al. (Pu et al., 2024). Moreover, the absorption band at about 1027 cm^{-1} indicating the formation of a shoulder for residual PO_4^{3-} as a result of unreacted Hap particles. Besides, an increase in this bandwidth was also due to the increasing distance between Si and O indicating the depolymerization of the network structure caused by the reduced fluidity due to less water and more powder which led to a thinner water film around each particle.

3.3.3. Morphology analysis

The morphology of Hap incorporated GMK25S1 is revealed in Fig. 7. In GMK25S1, the geopolymerization of S1 takes place on its surface with alkaline activator and with the dissolution of silica and alumina which participate in geopolymerization and gel formation. With the introduction of 1 % Hap, the geopolymer matrix was loose, the matrix distribution was uneven and with poor compactness caused by the incomplete binding which suggest lack of gel structure. In addition, the loose matrix structure demonstrating the geopolymer starts to form in discontinuous form offered more active sites for the adsorption of contaminants and greater removal rates. Apart from that, the large pores are visible in the geopolymer matrix were due to the greater amount of free water in agreement with FTIR analysis.

However, with the addition of 2 % of Hap, the geopolymer structure became more compact, massive gel appeared by the accelerated geopolymerization and the particles surface was covered by a gelatinous substance. The SAP and CASH gel formed on the tetrahedral SiO_4 of raw S1 and MK cemented the particles together which might be due to the abundant Si-OH groups on the surface of S1 and MK that facilitated the polycondensation. The formed gel filled the pores thereby the geopolymer structure became dense and porosity decreased with the development of interparticle binding phase. In contrast, the development of mesopores can be observed by the extent of geopolymerization as shown in Fig. 7(e-f). This is consistent with research conducted by Ren et al. (Ren et al., 2023) who suggested that the process of geopolymerization enriches the porosity of geopolymers, hence improving their nanopore properties and potentially increasing the number of contact and rich active sites available for adsorption.

On the other hand, the microstructure of GMK25S1-3Hap was relatively more disordered due to excessive Hap particles. This was due to an imbalance in the charge of the excess $[PO_4]^{3-}$ units caused by excess Hap addition, which made it difficult to be cured. As a result of the excess unreacted Hap that remained in GMK25S1-3Hap which was not conducive for the adsorption. Moreover, higher amount of Hap particles covers on MK and S1 particles and hinder the geopolymerization. Consequently, the gel network decreases with increasing the amount of Hap up to 3 % due to the low degree of geopolymerization. Thus, adequate adsorption performance of geopolymer could not be supported due to the low degree of reactivity and insufficiency of the hydration products.

3.3.4. Distribution of pores saturated water

Besides, neutron imaging has shown to be an effective non-destructive method to quantitatively evaluate the water content and water flow in porous materials. A neutron beam is much more attenuated by hydrogen in water than by most other elements present in geopolymer materials such as Si, Al, Ca and Na. Thus, the distribution of porosity saturated water in GMK25S1 sample with and without addition of Hap before curing can be elucidated by conducting neutron tomography imaging. In this work, the adsorption technique was carried out using GMK25S1-2Hap that had been oven-dried to 60 °C. Some of the free water from GMK25S1-2Hap has evaporated during the 60 °C curing process. However, as the CASH gel species in GMK25S1-2Hap goes through a slow and prolonged dehydration process up to 600 °C, the residual free water and chemical water were preserved in the mixture.

Therefore, a greater encapsulated water content was observed in GMK25S1-2Hap in comparison to GMK25S1 as the Hap content rose from 0 to 2 % demonstrating a significant increase of C-A-S-H gel as shown in Fig. 8 (d-f). This resulted from the enhancement of active CaO components in the geopolymers caused by the incorporation of Hap. When, the C-A-S-H reacts with water, it increases the basicity of the medium, which in turn influences the dissolution of MK and S1. Therefore, the dissolution rate of raw materials in alkaline activator to produce silica and alumina involved in the gel phase formation process was faster with the introduction of Hap, which had an increase in the formation of hydration products. In an alkaline environment, the dissolution of MK and S1 release SiO_2 and Al_2O_3 which further react with OH^- to form $[H_3SiO_4]^-$ and $[H_3AlO_4]^{2-}$ as monomers for the geopolymerization. Then, the $[H_3SiO_4]^-$ and $[H_3AlO_4]^{2-}$ react with Ca^{2+} in the system result in the substantial production of CASH gel in GMK25S1-2Hap (Yang et al., 2024). The greater generation of the CASH gel may provide an abundant of binding site containing active silicate and aluminate functional groups, which improve the complexation with Cu (II)/CIP from wastewater. In addition, majority of Cu(II) may occupy the Ca(II) sites in the interlayer pore during adsorption (Liu et al., 2023). Therefore, the variations in the CASH gel content strongly related to changes in the adsorption performance of geopolymer.

3.3.5. Textural properties

In addition, the nitrogen adsorption and desorption isotherm of geopolymers with and without addition of Hap are illustrated in Fig. 9. According to the International Union of Pure and Applied Chemistry (IUPAC) classification, the two tested samples revealed type-IV hysteresis loop in the P/Po region from 0.01 to 0.99, which are typical for mesoporous compounds. The GMK25S1 adsorbed an increased amount of N_2 compared to GMK25S1-2Hap, which satisfies its considerably higher surface area. However, as illustrated in Table 3, the inclusion of Hap significantly reduced the surface area of the GMK25S1-2Hap due to the blockage of matrix pores following possible intrusion of Hap nanoparticles into the MK and S1 mineral lattice or pores during the slurry preparation (Ashiq et al., 2019). Furthermore, it was found that a minor decrease in pore size was brought by the significant volumes of gel products produced by the raw materials worked synergistically under optimal Hap introduction which filled the pores and improved the geopolymer density.

Besides, pore size distributions of GMK25S1 and GMK25S1-2Hap are comparable, with the majority of pores measured less than 100 nm with a central peak at 26 nm. However, in GMK25S1-2Hap, the mesoporous (2–50 nm) range of 5–42 nm was found to have the largest fraction of pores. As illustrated in Fig. 10, these mesoporous were divided into gel pores with pore widths of (<10 nm) and capillary pores with pore widths of (>10 nm). The gel pores and capillary pores were introduced by the raw material and the geopolymer gels which were crucial components of

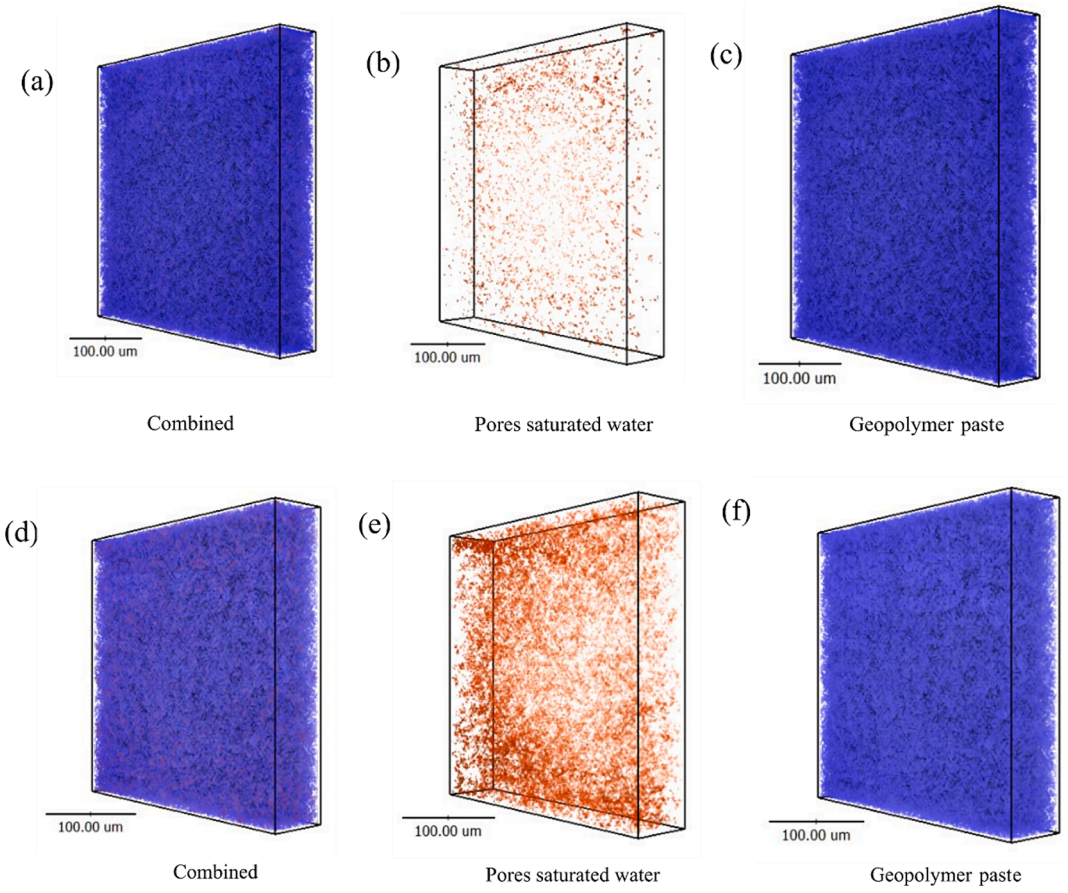

Fig. 8. Distribution of pores saturated water in geopolymer before curing, (a-c) GMK25S1 and (d-f) GMK25S1-2Hap.

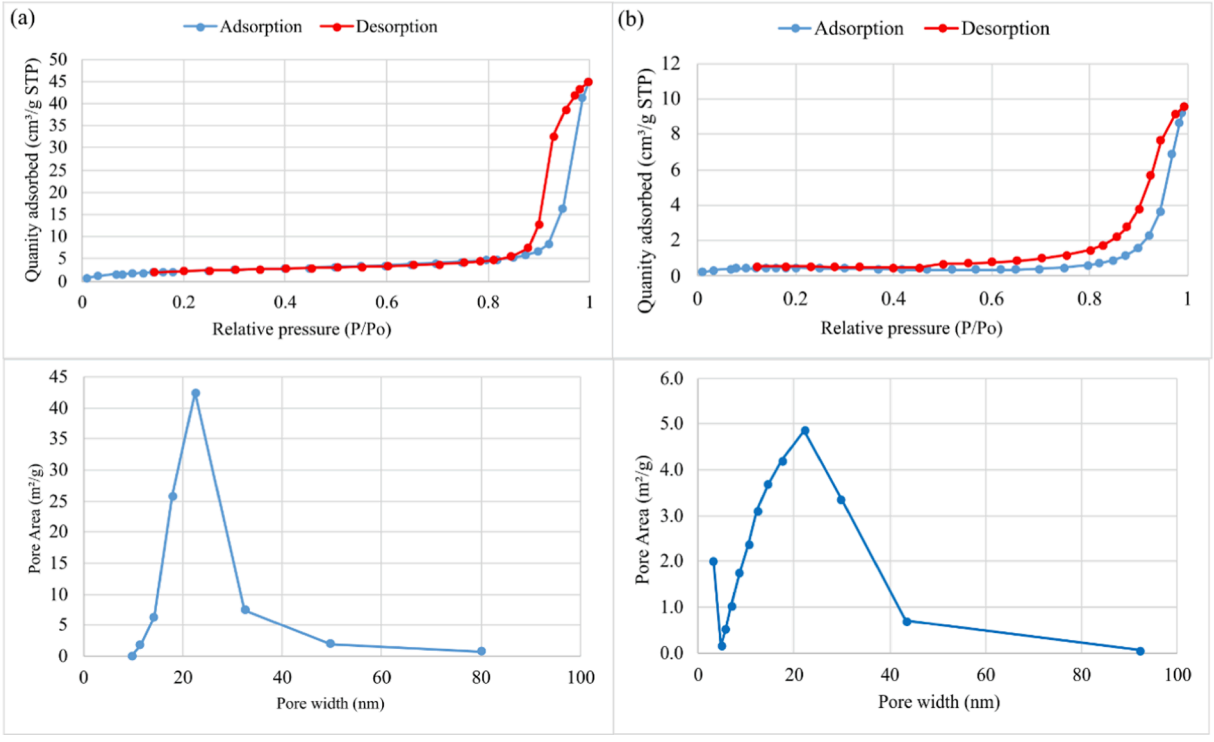

Fig. 9. N_2 adsorption and desorption isotherm and pore size distribution (a) GMK25S1, (b) GMK25S1-2Hap.

Table 3
BET surface area, pore volume and average pore size of geopolymers.

Sample	S_{BET} (m_2/g)	Pore volume (cm^3/g)	Average pore size (nm)
GMK25S1	8.86	−0.000951	28.8
GMK25S1-2Hap	1.58	0.00573	26.8

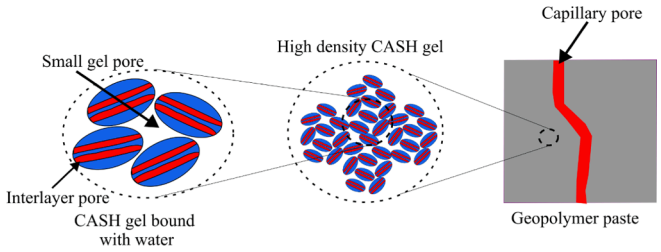

Fig. 10. Distribution of gel pores and capillary pores.

the structure of geopolymer. A study by Zhang et al. (Zhang et al., 2023) demonstrated that the capillary pore size might indicate the degree of reaction, with the highest fraction of gel pores found in fully reacted samples. Thus, the combination of high degree of geopolymerization and fully reacted samples in GMK25S1-2Hap was the main reason for the observed spike. The formation of mesopores will reduce the penetration resistance of geopolymer thereby increasing the adsorption performance of GMK25S1-2Hap. This explains the enhancement of adsorption performance after incorporation of Hap.

3.3.6. Adsorption mechanism of Cu(II)/CIP by GMK25S1-2Hap

The phase changes in GMK25S1-2Hap before and after adsorption of Cu(II)/CIP was analysed by XRD. As shown in Fig. 11, the main crystalline phases of GMK25S1-2Hap are berlinite, quartz, anorthite, akermanite and calcite. However, after adsorption, the peak intensities of the phases become weaker, indicating that they have been affected by the adsorption process. On the other hand, the crystal form and structure of the GMK25S1-2Hap had not changed considerably after adsorption since peak positions remain unchanged. This is consistent with a research conducted by Tunali et al. (Tunali et al., 2022), who suggested there is no change in the XRD spectra following Cu(II) adsorption as the Cu(II) adsorption by metakaolin-based geopolymer (MKG) is not expected to result in any phase changes in MKG or the creation of crystalline phases in species containing copper. This is because of an ion-exchange process that replaces Cu(II) ions in the MKG structure with Na(I) ions. The ion-exchange mechanism in the amorphous structure of geopolymers involves the straightforward replacement of one specific ion with another ion without resulting in any structural modifications. Moreover, following interaction with the Cu(II) and CIP-containing solution, a strong and sharp peak at 2θ of 11° was noticed, suggesting the formation of a new complex as a result of Cu(II)/CIP interacting with GMK25S1-2Hap. A similar finding was obtained in a study by Zhou et al. (Zhou et al., 2019), which highlighting the appearance of a minor peak at 2θ of 11° after coming in contact with the solution containing Cu(II) and norfloxacin. However, this peak appeared stronger in this study because of the improved adsorption of Cu(II)/CIP with higher capacity, produced high absorbance as predicted. Thus, based on the XRD analysis, it can be inferred that mechanisms such as ion exchange and complexation were involved in the Cu(II)/CIP removal.

On the other hand, the FTIR spectra of GMK25S1-2Hap before and after adsorption of Cu(II)/CIP in Fig. 12 was employed to illustrate the adsorption mechanism. The highlighted peaks in GMK25S1-2Hap have been displaced from their initial positions after Cu(II)/CIP loading, indicating the interactions between the relevant functional groups of the GMK25S1-2Hap and Cu(II)/CIP. Interestingly, the hydroxyl group (OH^-) of GMK25S1-2Hap at 3467 and 1640 cm^{-1} is moved to 3359 and 1638 cm^{-1}, respectively indicating the presence of hydrogen bonding. This

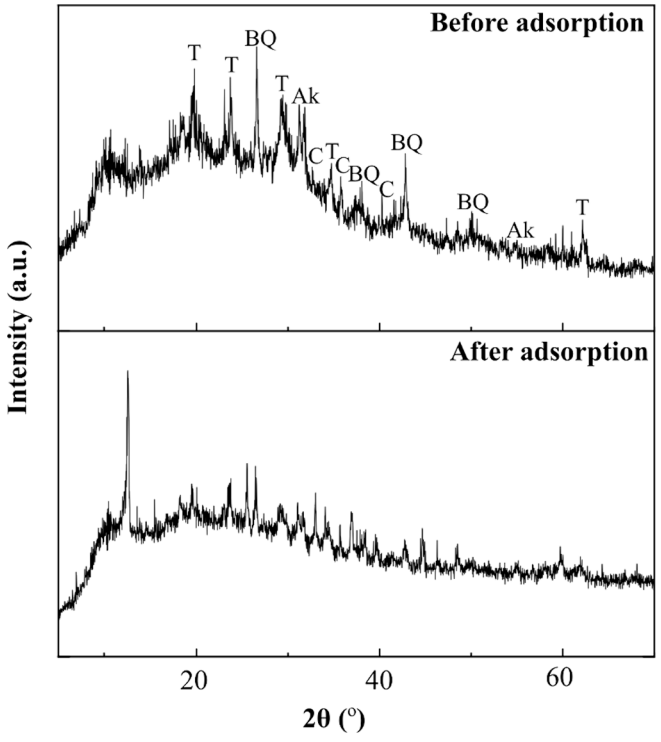

Fig. 11. XRD spectra of GMK25S1-2Hap before and after adsorption of Cu (II)/CIP.

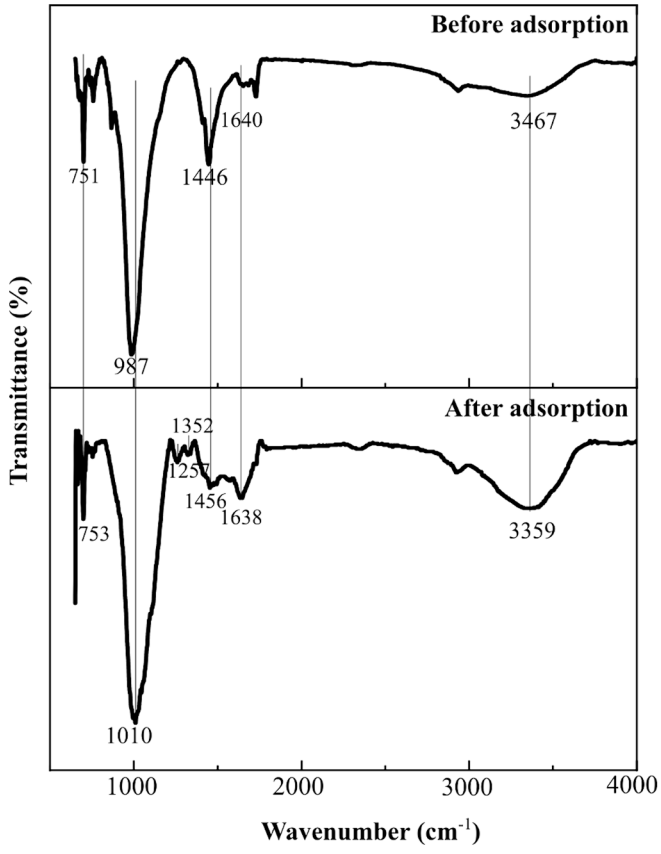

Fig. 12. FTIR spectra of GMK25S1-2Hap before and after adsorption of Cu (II)/CIP.

shift in frequency may be caused by the chemical coordination between Cu(II)/CIP and –OH, which lowers the electron cloud and modifies the vibration frequency of oxygen-containing functional group. Besides, the vibration frequency caused by the Si-O-T at 987 cm^{-1} at 751 cm^{-1} shifted to higher wavenumber after adsorption, possibly as a result of Cu^{2+} enrichment in GMK25S1-2Hap. Moreover, after interacting with the Cu(II) and CIP, two new peaks were observed at 1257 cm^{-1} and 1352 cm^{-1}, which correspond to the carboxyl acid ($–COO^-$) stretching vibrations and protonation of the amine group (HN_3^+) in the piperazine moiety of CIP, which demonstrated the complexation of Cu(II) with carboxyl group of CIP and hydrogen bonding between the nitrogen atoms (N) in the CIP structure and the hydrogen atoms (H) on the GMK25S1-2Hap surface. The H of the hydroxyl groups on the GMK25S1-2Hap surface act as H-donor and N of CIP, which act as H–acceptor have the strong possibility to form strong bonds which are called as dipole–dipole hydrogen bonding. Besides, the intensity of the peak related to calcite at 1446 cm^{-1} in GMK25S1-2Hap decreased sharply, suggesting calcite was involved in the reaction by forming complexation with CIP. Thus, the functional groups such as –OH, SiO^-, PO^-, AlO^- and CO^- play a crucial role in the Cu(II)/CIP adsorption.

Besides, the differences in the elemental distribution of GMK25S1-2Hap before and after exposure to Cu(II)/CIP were detected by using EDS analysis. Before adsorption, GMK25S1-2Hap mainly composed of Si (6.89 %), Al (2.39 %), P (1.60 %), Ca (4.49 %), Mg (1.79 %) and Na (3.54 %) as shown in Fig. 13(a). However, after adsorption, the most noticeable changes following exposure to contaminants was an increase in the N (4.30 %), F (0.92 %) and C (49.05 %) content, which indicating, the presence of CIP on the surface of GMK25S1-2Hap. In addition, the elemental composition of Ca, Mg and Na was dropped with an increase in the Cu (6.53 %) content on GMK25S1-2Hap, indicating Cu(II) adsorbed onto the surface of the adsorbent and exchanged with some of the alkali metal ions.

4. Comparison with previous studies

In a previous study by Yao et al. (Yao et al., 2023); iron and nitrogen co-doped rape straw derived biochar (Fe/N-BC), was used to adsorb Cu (II) and CIP in both single and binary systems. The Fe/N-BC has the superior adsorption performance for Cu(II) (20.51 mg/g) and CIP (17.3 mg/g) in single system, demonstrating Fe/N co-doping could significantly improve the adsorption capacity. The well-developed pore properties and plentiful oxygen functional groups following Fe and N modification exhibit improved adsorption performances towards CIP and Cu(II). However, the maximum adsorption capacity (q_{max}) for CIP and Cu(II) in binary system were lower than the single system indicating a strong competition between CIP and Cu(II) for the limited number of active sites on the Fe/N-BC surface. Besides, in another study by Sun et al. (Sun et al., 2014), the adsorption of CIP on activated carbon was improved with the presence of Ni(II) when the initial pH solution was between 3.4 and 6.5. Ni(II) interacted with CIP to create complexes that were easier to adsorbed on activated carbon (AC) surface due to their higher positive surface charge compared to CIP^0 and CIP^+. However, the sorption of CIP onto AC required a longer time (30 h) to reach equilibrium as the adsorption of organic molecules onto AC took longer to attain equilibrium than that of heavy metals. In contrast, the q_{max} of Cu (II) and CIP obtained by the synthesized GMK25S1-2Hap in this study is presented in Table 4. It can be observed that the q_{max} of Cu(II) by GMK25S1-2Hap was more significant than previous reported studies without compromising the removal efficiency of CIP.

5. Conclusion

In summary, Hap can be a valuable addition to geopolymer matrix, as it can improve the simultaneous adsorption of Cu(II) and CIP without compromising their workability. However, it is important to carefully optimize the Hap content that contribution to adsorption to obtain the efficient results. Based on the characterization techniques, the enhanced geopolymerization caused by the incorporation of 2 % Hap led to the development greater amorphous (CASH and SAP) gel phases and active sites such as (Si-OH, Al-OH, P-OH and HCO_3^-) in addition to the additional mesopores (gel and capillary pores) formation which could favour the simultaneous adsorption of Cu(II) and CIP. Moreover, the batch adsorption experiment showed that GMK25S1-2Hap could simultaneously remove 96.62 % of Cu(II) and 61.5 % of CIP in the binary system better than a single system. Besides, the effectiveness of CIP removal by GMK25S1-2Hap showed an increase ranging from 25.6 % to 61.51 %. with the increase in the concentration of Cu(II) from 0 to 100 mg/L. This enhancement can be attributed to the complexation and bridging effect between Cu(II) and CIP resulting in the formation of GMK25S1-2Hap-Cu (II)-CIP complexes. Besides, the electrostatic interaction between $[Cu(II)\text{-}CIP]^{2+}$ with the negatively charged GMK25S1-2Hap surfaces

Table 4
Comparison between the CIP and Cu(II) adsorption capacity from the literature.

Adsorbent	Pollutants	Qmax (mg/g)	References
Biochar	CIPCu(II)	10.0017.50	(Yao et al., 2023)
Fe-Biochar	CIPCu(II)	13.0014.00	(Yao et al., 2023)
Fe/N-BC	CIPCu(II)	17.3020.51	(Yao et al., 2023)
Activated carbon	CIPNickel	442.54.69	(Sun et al., 2014)
Corn stalk cellulose	SulfamethoxazoleCu (II)	4.4129.7	(Lun et al., 2023)
Geopolymer/Hap	CIPCu(II)	13.6864.4	This study

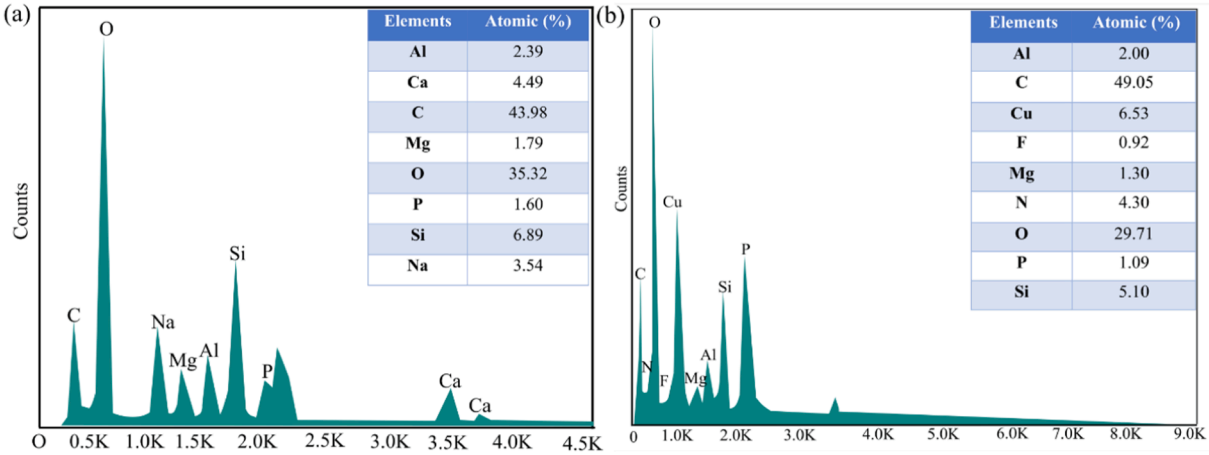

Fig. 13. EDS of GMK25S1-2Hap; (a) before and (b) after adsorption of Cu(II)/CIP.

increased the uptake of CIP due to high positive surface charge compared to CIP^0 and CIP^+. Therefore, GMK25S1-2Hap is a promising adsorbent for the elimination of combined pollution containing Cu(II) and CIP. Thus, this research offers a highly efficient and practical technique for simultaneously removing Cu(II) and CIP from contaminated wastewater.

CRediT authorship contribution statement

Pilomeena Arokiasamy: Writing – review & editing, Writing – original draft, Methodology, Investigation, Formal analysis, Conceptualization. **Mohd Mustafa Al Bakri Abdullah:** Writing – review & editing, Writing – original draft, Supervision, Project administration, Funding acquisition, Conceptualization. **Shayfull Zamree Abd Rahim:** Writing – review & editing, Supervision, Conceptualization. **Andrei Victor Sandu:** Validation, Project administration. **Anna Fedrigo:** Formal analysis, Data curation. **Ratna Ediati:** Writing – review & editing, Visualization, Validation. **Shafiq Ishak:** Writing – review & editing, Writing – original draft. **Noor Haida Mohd Kaus:** Writing – review & editing, Validation, Resources.

Declaration of Competing Interest

The authors declare that they have no known competing financial interests or personal relationships that could have appeared to influence the work reported in this paper.

Acknowledgments

The authors gratefully acknowledge the Ministry of Higher Education, Malaysia, through the Fundamental Research Grant Scheme (FRGS) under reference no. FRGS/1/2020/TK0/UNIMAP/01/2. The authors would like to acknowledge Geopolymer and Green Technology, Centre of Excellence (CEGeoGTech), University Malaysia Perlis (UniMAP), Faculty of Chemical Engineering Technology UniMAP, and ISIS Neutron and Muon Source.

References

Allaoui, D., Majdoubi, H., Haddaji, Y., Nadi, M., Mansouri, S., Oumam, M., Tamraoui, Y., Alami, J., Hannache, H., Manoun, B., 2023. Valorization of ceramic sanitary waste into resilient phosphoric acid-based geopolymers for sustainable construction: thermal, mechanical, and microstructural properties. Ceram. Int. https://doi.org/10.1016/j.ceramint.2023.12.203.

Arokiasamy, P., Mustafa, M., Bakri, A., Zamree, S., Rahim, A., Remy, M., Mohd, R., Zainol, A., Arif, M., Mohd, A., Kheimi, M., Chaiprapa, J., Victor, A., Vizureanu, P., Abdul, R., Hidayu, N., 2022. Case studies in construction materials metakaolin / sludge based geopolymer adsorbent on high removal efficiency of cu 2 +. Case Stud. Constr. Mater. 17, e01428.

Ashiq, A., Sarkar, B., Adassooriya, N., Walpita, J., Rajapaksha, A.U., Ok, Y.S., Vithanage, M., 2019. Sorption process of municipal solid waste biochar-montmorillonite composite for ciprofloxacin removal in aqueous media. Chemosphere 236, 124384. https://doi.org/10.1016/j.chemosphere.2019.124384.

Bambaeero, A., Bazargan-Lari, R., 2021. Simultaneous removal of copper and zinc ions by low cost natural snail shell/hydroxyapatite/chitosan composite, Chinese. J. Chem. Eng. 33, 221–230. https://doi.org/10.1016/j.cjche.2020.07.066.

Bazargan-Lari, R., Bahrololoom, M.E., Nemati, A., Salehi, Z., 2011. Adsorption of cu (II) ions from industrial wastewater on natural hydroxyapatite extracted from bone ash. J. Food Agric. Environ. 9, 652–657.

Bazargan-Lari, R., Bahrololoom, M.E., Nemati, A., 2011. Sorption behavior of zn (II) ions by low cost and biological natural hydroxyapatite/chitosan composite from industrial waste water. J. Food Agric. Environ. 9, 892–897.

Bazargan-Lari, R., Zafarani, H.R., Bahrololoom, M.E., Nemati, A., 2014. Removal of Cu (II) ions from aqueous solutions by low-cost natural hydroxyapatite/chitosan composite: equilibrium, kinetic and thermodynamic studies. J. Taiwan Inst. Chem. Eng. 45, 1642–1648. https://doi.org/10.1016/j.jtice.2013.11.009.

Cao, M., Liu, X., Wang, W., Gao, M., Yang, H., 2022. Bifunctional two-dimensional copper-aluminum modified filter paper composite for efficient tetracycline removal: synergy of adsorption and reusability by degradation. Chemosphere. 287, 132031 https://doi.org/10.1016/j.chemosphere.2021.132031.

Deng, J., Li, X., Wei, X., Liu, Y., Liang, J., Song, B., 2020. Hybrid silicate-hydrochar composite for highly e ffi cient removal of heavy metal and antibiotics : coadsorption and mechanism. Chem. Eng. J. 387, 124097 https://doi.org/10.1016/j.cej.2020.124097.

M. fang Li, Y. guo Liu, S. bo Liu, D. Shu, G. ming Zeng, X. jiang Hu, X. fei Tan, L. hua Jiang, Z. li Yan, X. xi Cai, Cu(II)-influenced adsorption of ciprofloxacin from aqueous solutions by magnetic graphene oxide/nitrilotriacetic acid nanocomposite: Competition and enhancement mechanisms, Chem. Eng. J. 319 (2017) 219–228. doi: 10.1016/j.cej.2017.03.016.

Feng, Y., Chen, G., Zhang, Y., Li, D., Ling, C., Wang, Q., Liu, G., 2022. Superhigh co-adsorption of tetracycline and copper by the ultrathin g-C3N4 modified graphene oxide hydrogels. J. Hazard. Mater. 424, 127362 https://doi.org/10.1016/j.jhazmat.2021.127362.

Ge, Y., Yuan, Y., Wang, K., He, Y., Cui, X., 2015. Preparation of geopolymer-based inorganic membrane for removing Ni2+from wastewater. J. Hazard. Mater. 299, 711–718. https://doi.org/10.1016/j.jhazmat.2015.08.006.

Hettithanthri, O., Rajapaksha, A.U., Keerthanan, S., Ramanayaka, S., Vithanage, M., 2022. Colloidal biochar for enhanced adsorption of antibiotic ciprofloxacin in aqueous and synthetic hydrolyzed human urine matrices. Chemosphere 297, 133984. https://doi.org/10.1016/j.chemosphere.2022.133984.

Hu, C., Jiang, J., An, Y., Jiang, X., Sun, Q., Zheng, H., 2022. A novel self-floating silica adsorbent for antibiotic ciprofloxacin and nickel (II) ion. Chem. Eng. J. 429, 132227 https://doi.org/10.1016/j.cej.2021.132227.

Jia, W.X., Li, W.Q., Xie, Z.H., Guo, P.C., Ye, Z.L., Xiong, Z.K., He, C.S., Lai, B., 2023. Adsorption behavior of antibiotics with different structures onto vivianite in the presence of dissolved organic matter during the phosphorus recovery process. Chem. Eng. J. 470, 144136 https://doi.org/10.1016/j.cej.2023.144136.

Jiang, B., Lin, Y., Mbog, J.C., 2018. Biochar derived from swine manure digestate and applied on the removals of heavy metals and antibiotics. Bioresour. Technol. 270, 603–611. https://doi.org/10.1016/j.biortech.2018.08.022.

D. Joseph, Geopolymer CHemistry and Applications, 5th edition, 2008. https://www.researchgate.net/publication/265076752.

Khurana, P., Pulicharla, R., Kaur Brar, S., 2021. Antibiotic-metal complexes in wastewaters: fate and treatment trajectory. Environ. Int. 157, 106863 https://doi.org/10.1016/j.envint.2021.106863.

Laabd, M., Brahmi, Y., El Ibrahimi, B., Hsini, A., Toufik, E., Abdellaoui, Y., Abou Oualid, H., El Ouardi, M., Albourine, A., 2021. A novel mesoporous hydroxyapatite@montmorillonite hybrid composite for high-performance removal of emerging ciprofloxacin antibiotic from water: integrated experimental and Monte Carlo computational assessment. J. Mol. Liq. 338, 116705 https://doi.org/10.1016/j.molliq.2021.116705.

Le, T.M.D., Dinh, T.D., Tran, T.M.H., Nguyen, M.K., Hoang, H., Vu, L.K., Vu, N.D.Q., Pham, T.D., 2024. Adsorption characteristics of individual and binary mixtures of ciprofloxacin antibiotic and Cu(II) on nanosilica in water. J. Mol. Liq. 398, 124298 https://doi.org/10.1016/j.molliq.2024.124298.

Li, M., Liu, Y., Liu, S., Shu, D., Zeng, G., Hu, X., 2017. Cu (II) -influenced adsorption of ciprofloxacin from aqueous solutions by magnetic graphene oxide / nitrilotriacetic acid nanocomposite : competition and enhancement mechanisms. Chem. Eng. J. 319, 219–228. https://doi.org/10.1016/j.cej.2017.03.016.

Ling, C., Zhao, Y., Ren, Z., Han, J., Zhu, C., Liu, F.Q., 2019. Synergistic co-removal of zinc (II) and cefazolin by a Fe/amine-modified chitosan composite. Chinese Chem. Lett. 30, 2196–2200. https://doi.org/10.1016/j.cclet.2019.09.035.

Liu, Q., Feng, P., Shao, L., Liu, X., Chen, C., Lu, J., Ling, C., Zhang, Y., Sun, D., Ran, Q., 2023. Ultra-purification of heavy metals and robustness of calcium silicate hydrate (C–S–H) nanocomposites. Chemosphere. 335, 139063 https://doi.org/10.1016/j.chemosphere.2023.139063.

Louati, S., Baklouti, S., Samet, B., 2016. Acid based geopolymerization kinetics: effect of clay particle size. Appl. Clay Sci. 132–133, 571–578. https://doi.org/10.1016/j.clay.2016.08.007.

Lun, L., Su, Y., Gong, X., Zhang, L., Meng, P., Peng, D., Zhou, Q., Zeng, H., Zheng, L., 2023. Co-adsorption and competitive adsorption of sulfamethoxazole by carboxyl-rich functionalized corn stalk cellulose in the presence of heavy metals. Ind. Crops Prod. 199, 116761 https://doi.org/10.1016/j.indcrop.2023.116761.

Lv, M., Zhang, T., Ya, H., Xing, Y., Wang, X., Jiang, B., 2023. Effects of heavy metals on the adsorption of ciprofloxacin on polyethylene microplastics: mechanism and toxicity evaluation. Chemosphere. 315, 137745 https://doi.org/10.1016/j.chemosphere.2023.137745.

Ma, J., Xiong, Y., Dai, X., Yu, F., 2020. Coadsorption behavior and mechanism of ciprofloxacin and Cu(II) on graphene hydrogel wetted surface. Chem. Eng. J. 380, 122387 https://doi.org/10.1016/j.cej.2019.122387.

Ma, J., Xiong, Y., Dai, X., Yu, F., 2020. Coadsorption behavior and mechanism of cipro fl oxacin and Cu (II) on graphene hydrogel wetted surface. Chem. Eng. J. 380, 122387 https://doi.org/10.1016/j.cej.2019.122387.

Ma, S., Zhang, Z., Liu, X., 2022. Comprehensive understanding of aluminosilicate phosphate Geopolymers: a critical review. Materials (basel). 15 https://doi.org/10.3390/ma15175961.

Petlitckaia, S., Barré, Y., Piallat, T., Grauby, O., Ferry, D., Poulesquen, A., 2020. Functionalized geopolymer foams for cesium removal from liquid nuclear waste. J. Clean. Prod. 269 https://doi.org/10.1016/j.jclepro.2020.122400.

Pooladi, A., Bazargan-Lari, R., 2020. Simultaneous removal of copper and zinc ions by chitosan/hydroxyapatite/nano-magnetite composite. J. Mater. Res. Technol. 9, 14841–14852. https://doi.org/10.1016/j.jmrt.2020.10.057.

Pooladi, A., Bazargan-Lari, R., 2023. Adsorption of zinc and copper ions simultaneously on a low-cost natural chitosan/hydroxyapatite/snail shell/nano-magnetite composite. Cellulose. 30, 5687–5705. https://doi.org/10.1007/s10570-023-05219-3.

Pu, S., Shen, Z., Wu, Z., Yao, H., Xu, B., Zhu, Z., Duan, W., 2024. Enhancement mechanical properties of phosphoric-based geopolymer using aluminum dihydrogen phosphate. Mater. Today Commun. 38, 107656 https://doi.org/10.1016/j.mtcomm.2023.107656.

Ren, Z., Zhang, C., Zhao, F., Meng, J., Han, X., Liang, J., 2023. Synthesis of phosphoric acid-based mesoporous geopolymers from tourmaline tailings for effective adsorption of tetracycline hydrochloride in aqueous environment. Microporous Mesoporous Mater. 362, 112786 https://doi.org/10.1016/j.micromeso.2023.112786.

Sha, J., Li, L., An, Z., He, M., Yu, H., Wang, Y., Gao, B., Xu, S., 2022. Diametrically opposite effect of Cu2+ on sulfamerazine and ciprofloxacin adsorption-photodegradation in g-C3N4/visible light system: behavior and mechanism study. Chem. Eng. J. 428, 131065 https://doi.org/10.1016/j.cej.2021.131065.

Sha, J., Li, L., An, Z., He, M., Yu, H., Wang, Y., Gao, B., Xu, S., 2022. Diametrically opposite effect of cu 2 + on sulfamerazine and ciprofloxacin adsorption-photodegradation in g-C 3 N 4 / visible light system : behavior and mechanism study. Chem. Eng. J. 428, 131065 https://doi.org/10.1016/j.cej.2021.131065.

Sun, Y., Yue, Q., Gao, B., Gao, Y., Xu, X., Li, Q., Wang, Y., 2014. Adsorption and cosorption of ciprofloxacin and Ni(II) on activated carbon-mechanism study. J. Taiwan Inst. Chem. Eng. 45, 681–688. https://doi.org/10.1016/j.jtice.2013.05.013.

Tunali, S., Çolo, H., Sayin, F., Kara, I., Akar, T., 2022. Parametric optimization of cu (II) removal process by a metakaolin-based geopolymer : batch and continuous process design. J. Clean. Prod. 366, 132819 https://doi.org/10.1016/j.jclepro.2022.132819.

Wagh, A.S., 2016. Chemically bonded phosphate ceramic matrix composites. Chem. Bond. Phosphate Ceram. 179–201. https://doi.org/10.1016/b978-0-08-100380-0.00014-2.

Wang, R.Z., Huang, D.L., Liu, Y.G., Zhang, C., Lai, C., Wang, X., Zeng, G.M., Zhang, Q., Gong, X.M., Xu, P., 2020. Synergistic removal of copper and tetracycline from aqueous solution by steam-activated bamboo-derived biochar. J. Hazard. Mater. 384, 121470 https://doi.org/10.1016/j.jhazmat.2019.121470.

Wang, M., yi You, X., 2023. Efficient adsorption of antibiotics and heavy metals from aqueous solution by structural designed PSSMA-functionalized-chitosan magnetic composite. Chem. Eng. J. 454, 140417 https://doi.org/10.1016/j.cej.2022.140417.

Xu, Z., Huang, W., Wang, S., Song, H., Xu, J., Mailhot, G., Tong, Z., Zhang, H., Li, Z., 2023. Journal of environmental chemical engineering co-adsorption characteristics of antibiotics with different functional groups and cadmium combined contamination on activated carbon. J. Environ. Chem. Eng. 11, 110070 https://doi.org/10.1016/j.jece.2023.110070.

Yang, X., Wu, S., Xu, S., Chen, B., Chen, D., Wang, F., Jiang, J., Fan, L., Tu, L., 2024. Effects of GBFS content and curing methods on the working performance and microstructure of ternary geopolymers based on high-content steel slag. Constr. Build. Mater. 410, 134128 https://doi.org/10.1016/j.conbuildmat.2023.134128.

Yao, B., Zeng, W., Núñez-Delgado, A., Zhou, Y., 2023. Simultaneous adsorption of ciprofloxacin and Cu2+ using Fe and N co-doped biochar: competition and selective separation. Waste Manag. 168, 386–395. https://doi.org/10.1016/j.wasman.2023.06.014.

Zhang, J., Fu, Y., Wang, A., Dong, B., 2023. Research on the mechanical properties and microstructure of fly ash-based geopolymers modified by molybdenum tailings. Constr. Build. Mater. 385, 131530 https://doi.org/10.1016/j.conbuildmat.2023.131530.

Zhao, R., Ding, W., Sun, M., Yang, L., Liu, B., Zheng, H., Li, H., 2022. Insight into the co-removal of Cu(II) and ciprofloxacin by calcite-biochar composite: enhancement and competition. Sep. Purif. Technol. 287, 120487 https://doi.org/10.1016/j.seppur.2022.120487.

Zhou, L., Li, N., Owens, G., Chen, Z., 2019. Simultaneous removal of mixed contaminants, copper and norfloxacin, from aqueous solution by ZIF-8. Chem. Eng. J. 362, 628–637. https://doi.org/10.1016/j.cej.2019.01.068.

Zhou, Z., Sun, Y., Wang, Y., Yu, F., Ma, J., 2022. Chemosphere adsorption behavior of Cu (II) and Cr (VI) on aged microplastics in antibiotics-heavy metals coexisting system. Chemosphere 291, 132794. https://doi.org/10.1016/j.chemosphere.2021.132794.